ACS Photonics

pubs.acs.org/journal/apchd5 Article

Ultrafast Control of the Optical Transition in Type-II Colloidal Quantum Wells

Junhong Yu,* Emek Goksu Durmusoglu, Yimeng Wang, Manoj Sharma, Hilmi Volkan Demir,* and Cuong Dang*

Cite This: *ACS Photonics* 2023, 10, 1250−1258 Read Online

ACCESS | Metrics & More | Article Recommendations | Supporting Information

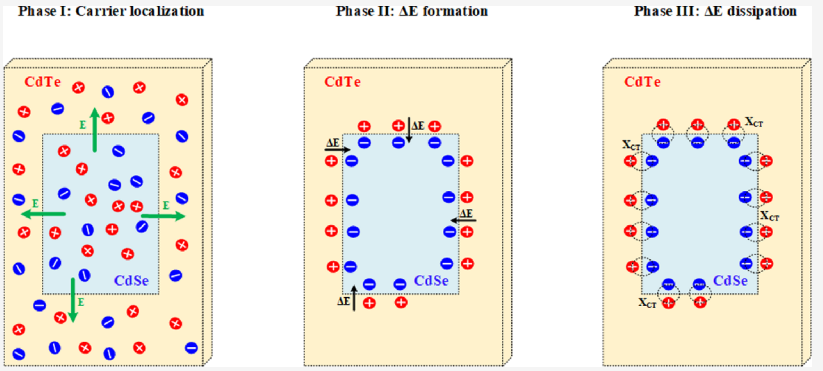

ABSTRACT: Manipulating the optical transition in semiconductors at ultrashort timescales is of both fundamental interest and central importance for emerging photonic applications. Traditionally, this manipulation is realized by electrostatic gating via Stark effects or band-gap renormalizations. Here, we report an ultrafast and all-optical route to engineer an indirect transition in core−crown colloidal quantum wells (CQWs), namely, CdSe/CdTe, with a type-II band alignment. Following the intense laser pulse excitation, the indirect band transition energy exhibits a pronounced blueshift−redshift crossover on the picosecond timescale, stemming from the formation and dissipation of the transient electric field (E-field) that forms upon photoexcitation to compensate for the driving force provided by the band offsets. Both the energy shift and dynamics of the transient E-field can be modulated optically by tuning the laser pulse excitation fluence. Our finding demonstrates a strong analogy between the type-II heterojunction and a p−n junction with respect to carrier equilibrium processes, which holds promise to facilitate the integration of CQWs within optical switching networks.

KEYWORDS: *colloidal quantum wells, type-II heterojunction, ultrafast spectroscopy, optical modulation, CdSe/CdTe*

INTRODUCTION

The investigation and manipulation of optical transition in semiconductors are important topics in condensed matter physics[1,2] and underlie future photonic applications, including optical switching and modulating.[3] To date, successfully demonstrated manipulation schemes[4−10] mostly rely on the Stark effect (i.e., the band is tilted to oppose the external E-field) or the band-gap renormalization due to electrostatic doping (i.e., the free carriers modify the electrostatic energies to shift the conduction and valence band toward each other). However, these approaches cannot go beyond the limitations of electronics and strongly hinder the practical applications in integrated circuits due to sacrificing the operation speed and the restriction in the modulation depth. To tackle this issue, all-optical manipulation is one of the most fascinating directions that offers high-speed processing and versatile modulation capability.[11−13] Although pioneer works have demonstrated temporally manipulating various optical properties (e.g., refractive index,[11] carrier temperature,[12] and electroabsorption[13]) in colloidal nanocrystals, ultrafast control of optical transitions in colloidal nanocrystals is still a daunting challenge.

Recent advances in colloidal quantum wells (CQWs), particularly those CQWs with a fully type-II band alignment (i.e., the conduction band minimum and valence band maximum are residing in two different domains), offer a unique platform to investigate the all-optical manipulation.[14−20] In type-II CQWs (e.g., CdSe/CdTe CQWs), when photo-generated excitons/carriers in either domain of the

Received: November 16, 2022
Published: April 21, 2023

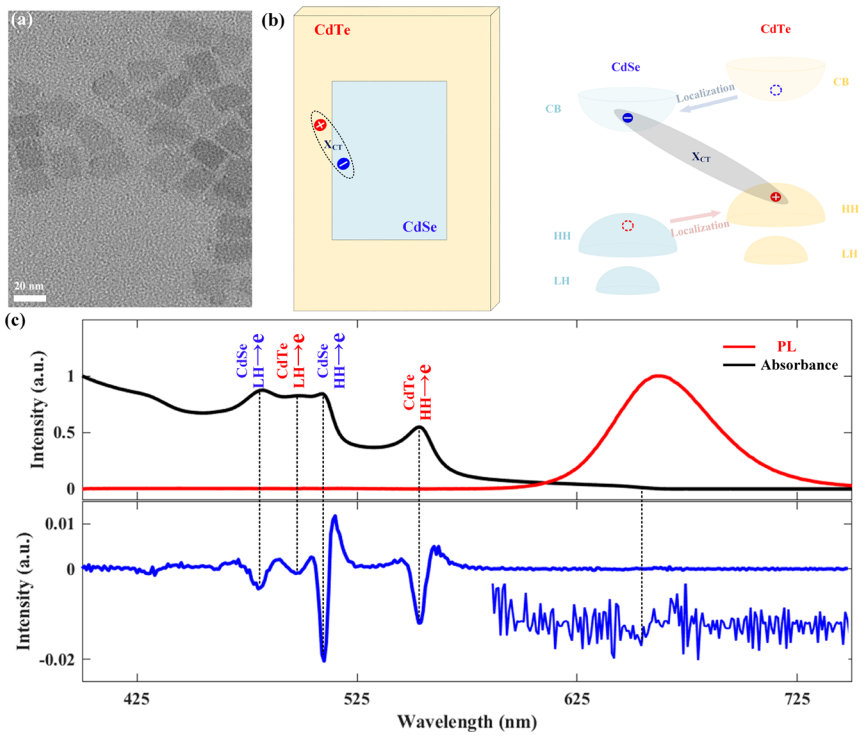

Figure 1. Band alignment and structure of CdSe/CdTe type-II CQWs. (a) Transmission electron microscopy (TEM) images of the synthesized 4-ML core−crown CdSe/CdTe CQWs with an overall size of ∼22 nm × 36 nm. (b) Schematic illustrations of the core−crown structure (left panel) and the predicted band alignment (right panel) with a fully type-II heterojunction. Photogenerated carriers/excitons in both CdSe and CdTe domains will be localized to the interface with electrons in CdSe and holes in CdTe. These domain-separated electrons and holes have a chance to form the charge transfer excitons (X_{CT}). CB: conduction band, HH: heavy hole, and LH: light hole. (c) Absorption (black) and photoluminescence (red) spectra of CdSe/CdTe CQWs. Absorption second derivative (blue) spectra of the type-II CQWs are also presented to help determine the possible transition energies. Inset of bottom panel: a zoom-in of the second derivative curve to show the charge-transfer (CT) state.

heterojunction diffuse to the interface, ultrafast charge transfer (CT), which occurs in the femtosecond timescale, generates electrons and holes separated in different domains. This gives rise to the n-doping and p-doping for CdSe and CdTe, respectively.[14,21] Benefitting from the strong Coulombic interactions due to quantum confinement and reduced dielectric screening in these few-monolayer thick CQWs, electrons/holes across the interface create a considerable transient E-field to oppose the further charge separation where the driving force is provided by the band offsets.[12,22] Therefore, in close analogy to the carrier equilibrium process in the p−n junction or the band bending in organic photovoltaics,[23] the build-up and dissipation of the photogenerated transient E-field in type-II CQWs provide a good opportunity to examine the all-optical control of band transition in semiconductors. However, despite several studies addressing the dynamics of excitons and carrier separation in type-II CQWs,[14−16,18,24,25] the role of the photogenerated transient E-field on optical transition remains unexplored experimentally.

Herein, we demonstrate the crossover control of the optical transition at nano-heterojunctions in CdSe/CdTe CQWs on the ultrafast timescale using time-resolved (TR) absorbance spectroscopy. In particular, after the intense femtosecond optical excitation (e.g., 2164 $\mu J/cm^2$ at 410 nm), we observe a pronounced blueshift (∼72 meV) of the indirect band transition energy at the early time stage (with a lifetime of ∼4.51 ps) followed by a faster redshift (with a lifetime of ∼1.21 ps), which almost recovers the indirect band transition energy to the static value. We attribute these two different energy shifts to the formation and decay process of the photogenerated transient electric field (E-field). Meanwhile, we further demonstrate that the manipulation of optical transition can be photo-controlled by varying the excitation fluence and the blueshifted energy linearly increases with the cube root of the exciton fluence, supporting again that the control of optical transition is caused by the transient E-field, which is generated by the separation of opposite charges across the interface. Our results may stimulate the future development of all-optical solid-state devices.

RESULTS AND DISCUSSION

Four-monolayer (∼1.4 nm in the vertical confinement direction) CdSe/CdTe core−crown CQWs, as shown in Figure 1a, are synthesized using a previous method with slight modifications (see details in the Methods).[19] These CQWs display rectangular shapes and crystallize in a zinc-blend structure with a CdTe crown grown on the facets of the CdSe core.[20] The band alignment of the core−crown CQWs is illustrated in Figure 1b, showing that the conduction band minimum resides in CdSe and the valence band maximum (i.e., the highest energy level for heavy holes) is located in CdTe. Consequently, the CdSe/CdTe CQW forms a type-II heterojunction with a conduction band and a valence band offset of 0.35 and 0.54 eV, respectively.[26] In the single-particle picture, this type-II heterostructure, driven by the band offsets, will lead to separated electrons and holes in two different domains upon photon excitation, forming an analogous p−n junction at the interface (i.e., CdSe is n-doping, and CdTe is p-doping).[23,27,28] The absorption and photoluminescence (PL)

https://doi.org/10.1021/acsphotonics.2c01799
ACS Photonics 2023, 10, 1250−1258

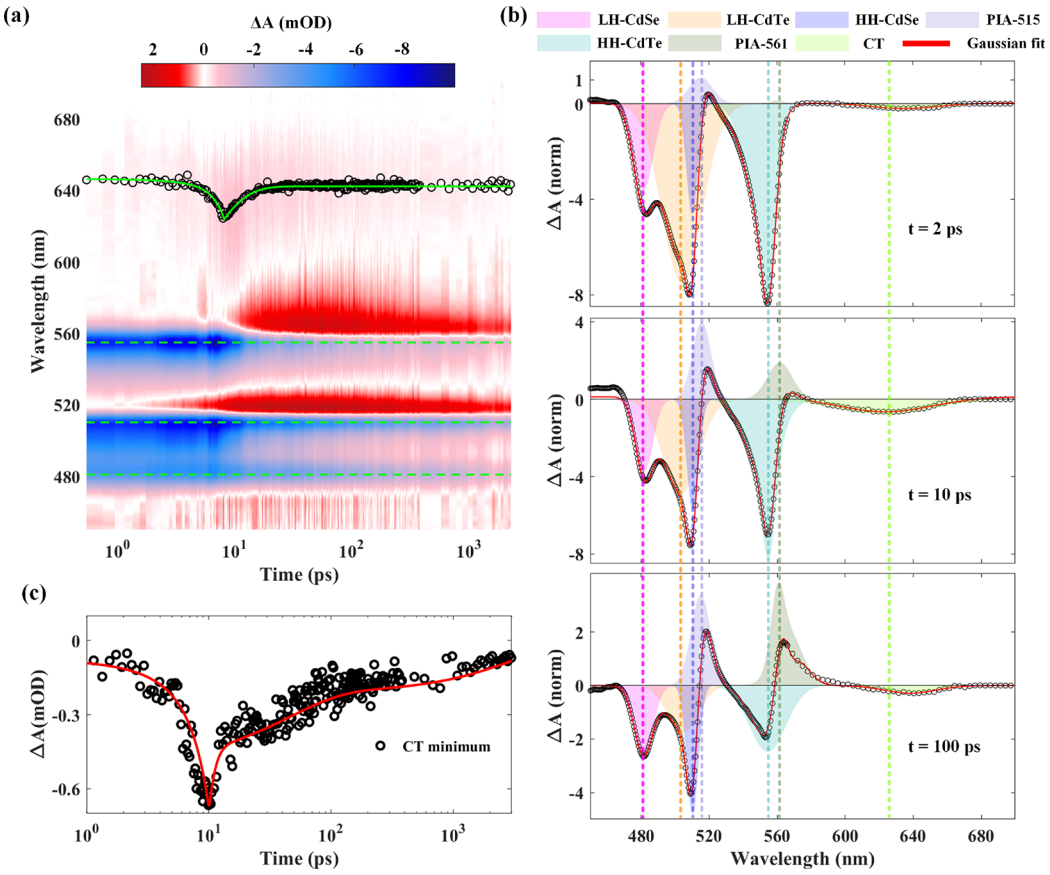

Figure 2. Time-resolved absorbance spectroscopy of CdSe/CdTe CQWs with an excitation fluence of 2164 μJ/cm^2 ($\langle N_{e-h}\rangle$: ~417). (a) Pseudocolor plot at room temperature. The horizontal axis, vertical axis, and color scale represent the pump−probe time delay, probe photon energy, and transient absorption signal, respectively. Three green dashed lines mark the peak wavelength of the direct transitions in CdSe and CdTe domains. The black dots indicate the wavelength position of the bleaching peak of the CT state extracted by Gaussian fittings, and the green curve is an exponential fitting. (b) Transient absorption spectra at three representative pump−probe delays, which are fitted by multiple Gaussian functions to determine the peak positions. The vertical dotted lines are located at the peak positions of corresponding transition bands when t = 10 ps. (c) Decay kinetics probed at the minimum wavelength of the CT state. Black dots: measurements. Red curve: exponential fitting.

spectra of as-prepared CdSe/CdTe CQWs dispersed in hexane are presented in Figure 1c. Typically, in type-II heterostructures (quantum dots,[29,30] nanorods,[31,32] or transition-metal dichalcogenides[12,27,33]), the absorption spectrum will exhibit both intra- and interdomain transition features. As shown in the black curve, four intradomain excitonic states centered at 480, 512, 501, and 560 nm can be well resolved, which correspond to the transitions associated with light holes (LHs) in CdSe, heavy holes (HHs) in CdSe, LHs in CdTe, and HHs in CdTe, respectively. Since the strength of the interdomain transition is very weak (i.e., the interfacial CT transition is indirect), the absorption spectrum lacks a pronounced feature related to the CT state. To quantify the static energy position of the interdomain transition, we analyze the second derivative of the absorption spectrum (the blue curve) and infer that the CT transition is located at ~646 nm (see the zoomed-in part).

While for the emission spectrum (the red curve in Figure 1c), the dominated radiative recombination from CT excitons (peaked at 662 nm) and the fully quenched emission from each domain (expected at ~512 nm for CdSe and ~556 nm for CdTe) have indicated a very effective charge separation. Recently, several reports[14−16,18,24] have investigated CT dynamics at the domain interface of CdSe/CdTe CQWs; although the role of the carrier interaction/excitonic effect on the charge separation process and how carriers across different domains can conserve the momentum are still under debate, a consensus from all reports is that interfacial CT occurs with near-unity efficiency and on an ultrafast sub-picosecond timescale (e.g., 0.48 ps in ref 14 and 70 fs in ref 16. We have also noticed that the CT emission shows a large Stokes shift (~16 nm) and broad linewidth (full width at half maximum: ~54 nm), which are in stark contrast to the nearly vanishing Stokes shift (2−4 nm) and the narrow emission (8−12 nm) in single-domain CQWs with atomic monolayer thickness confinement.[13,17] This is another fingerprint of fully type-II band alignment since the spatially separated electrons/holes are more polarizable and can heavily interact with longitudinal optical phonons through Frolich interactions.[34] In addition, we observe an averaged interdomain exciton lifetime of ~54.6 ns via the time-resolved PL measurement (see Figure S1), which is an order of magnitude longer than in intradomain excitons, again supporting the effective charge separation since the spatially indirect nature leads to a reduced electron/hole wavefunction overlapping.[25,33]

To probe whether excitation-generated carriers can affect optical transitions in type-II CQWs, we have measured transient absorption (TA) spectra using the pump−probe technique. We start with a weak excitation at 410 nm (0.6 μJ/cm^2, which corresponds to the number of generated electron−

https://doi.org/10.1021/acsphotonics.2c01799
ACS Photonics 2023, 10, 1250−1258

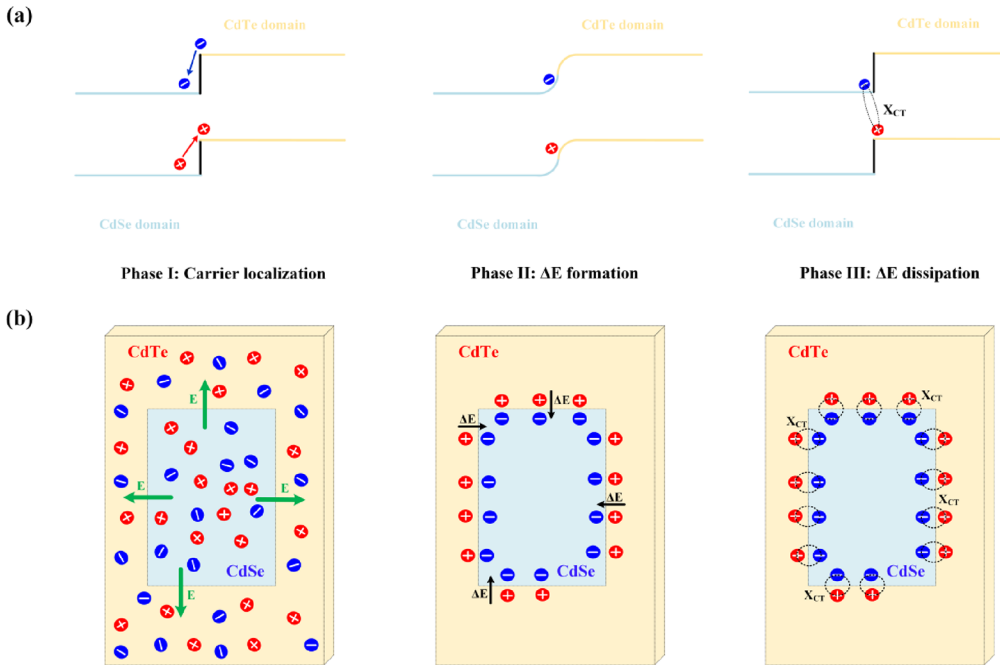

Figure 3. Schematic illustration of the optical transition modulation processes in CdSe/CdTe CQWs with (a) "energetic" and (b) "spatial" representations. In phase I, after photoexcitation, when the generated carriers/excitons diffuse to the interface, driven by the band offsets, the electrons and holes will be separately localized in CdSe and CdTe domains, respectively. In phase II, the electron/hole charge separation across the interface leads to a transient E-field build-up, which compensates for the band offsets and opposes the charge separation process. While in phase III, when carriers approach an equilibrium, these separated charges are bounded into the CT excitons. Therefore, $\Delta\varepsilon$ disappears due to these neutral excitons. Note that we do not depict the domain excitons in these schematics for clarity.

hole pairs, $\langle N_{e-h}\rangle$: ~0.01, see the Methods) to avoid any multi-carrier/exciton effects. As presented in Figure S2a, four intradomain and one interdomain bleaching band can be seen in the TA spectrum at the initial delay time (i.e., 2 ps) with energy locations agreeing well with that extracted from the steady-state absorption spectrum (Figure 1c). Meanwhile, based on the bleaching dynamics in Figure S2b, we can extract the carrier transfer lifetime (i.e., the separation time of electrons and holes in two different domains) as ~0.47 ps, agreeing well with previous reports.[14−16,18,24] Next, we focus on the multi-carrier scenario in CdTe/CdSe CQWs with high excitation densities. Figure 2a shows the transient absorption signals in false colors after an excitation fluence of 2164 μJ/cm^2 ($\langle N_{e-h}\rangle$: ~417), and the data reveal two distinct behaviors for inter- and intradomain transitions after performing multiple Gaussian fittings.[5] For CdSe-LH/-HH and CdTe-HH, the transition energy remains almost constant in the measured time window (as indicated by the green dashed lines; also see the extracted peak positions in Figure S3). In contrast, the CT transition band blueshifts gradually on the first ~10 ps after photoexcitation. At later times (i.e., after ~10 ps), the blueshift trend diminishes and turns into a redshift, which eventually restores the CT transition energy to the static value (i.e., 646 nm). This observation can be appreciated better by looking at three different spectral cuts (Figure 2b) with the delay time right at the shift turning point (blue curve) and before (green curve) and after (red curve) the shift turning point. For a quantitative analysis of the CT transition energy, we have depicted the energetic peak position for each spectral cut in Figure 2a (black circles), which shows that the maximum energy shift for a CT transition crossover is ~23 nm (~72 meV). More importantly, the transition crossover dynamics can be extracted by exponentially fitting the peak energy trace of the CT state, which reveals an averaged blueshift lifetime of ~3.85 ps and an averaged redshift lifetime of ~17.23 ps.

Due to the lack of a phonon bottleneck (the hot carrier relaxes within 100 fs),[8,35] the relatively slow carrier recombination rate (>50 ns), and the ultrafast charge transfer rate (<1 ps) in CdSe/CdTe CQWs, we can further check the CT transition crossover dynamics by analyzing bleaching signals at the minimum CT transition wavelength (i.e., 623 nm). As shown in Figure 2c, the bleaching dynamics at 623 nm can be well described by a single-exponential build-up process with a lifetime of ~4.51 ps and a bi-exponential recovery process with time constants of ~1.21 ps and ~3.47 ns. Comparing the time trace of peak energies presented in Figure 2a with the bleaching dynamics shown in Figure 2c, we can conclude that (i) the blueshift−redshift crossover (at ~9.54 ps in Figure 2a) occurs at the same time as the maximum bleaching signal (at ~10.12 ps in Figure 2c) and (ii) the build-up lifetime of bleaching dynamics (~4.51 ps in Figure 2c) is consistent with the blueshifting time constant (~3.85 ps in Figure 2a). These coincidences have verified the determining process of the CT energy-shifting dynamics and implied that the observed CT transition crossover is highly related to the photo-induced carrier/exciton dynamics. It should be noted that the recovery process extracted from the bleaching dynamics at 623 nm deviates from the redshifting kinetics in the time trace of peak energies, which can be understood as follows: (i) The slow recovery process with a lifetime of ~3.47 ns is close to the fast decay channel resolved in the time-resolved PL measurement (see Figure S1), which can be related to the recombination of interdomain excitons (X_{CT}). Please note that the time trace of peak locations reflects the change of CT transition energy and has a negligible connection with exciton recombinations; as a result, the slow recovery

https://doi.org/10.1021/acsphotonics.2c01799
ACS Photonics 2023, 10, 1250−1258

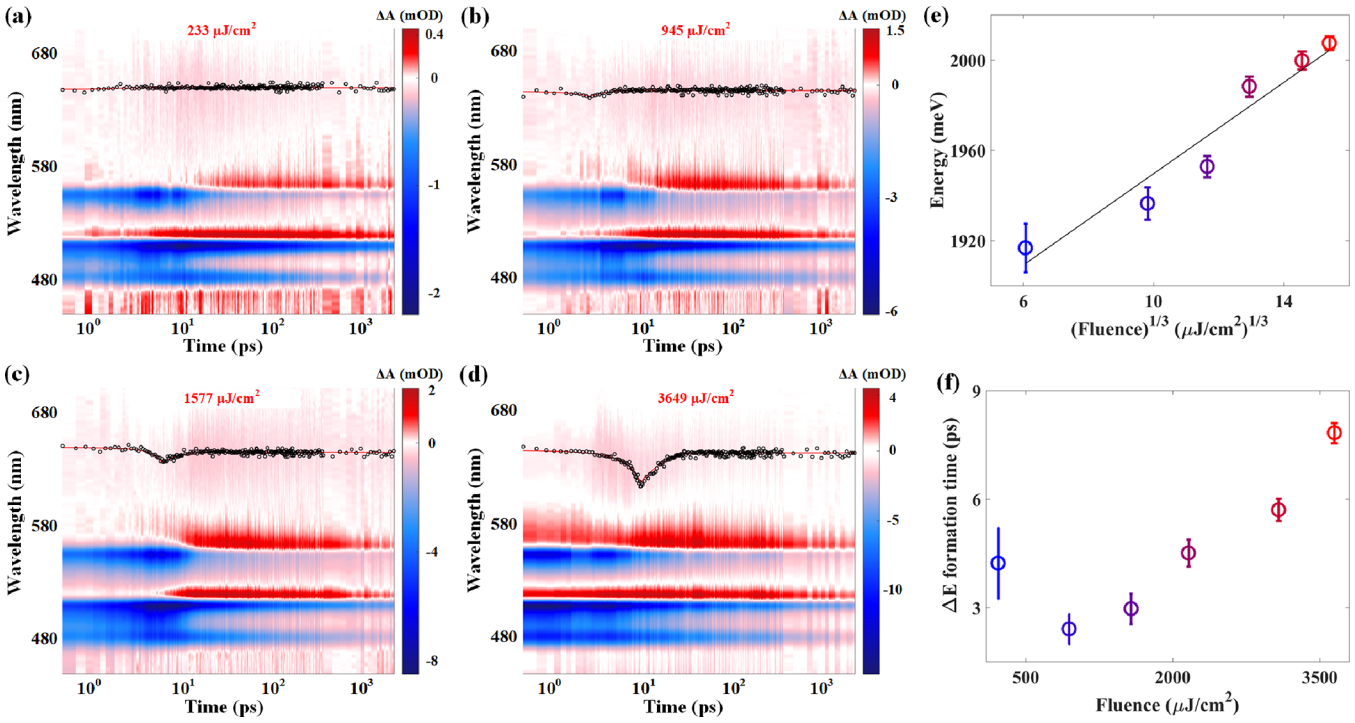

Figure 4. Optical transition crossover following various excitation fluences. (a–d) Pseudocolor plots of TR absorbance spectroscopy at increasing excitation fluences. The black dots indicate the wavelength position of the bleaching peak of the CT state. (e) Blue-shifted energy of the CT states as a function of the cubic root of the excitation fluence. The solid line is a linear fitting, and the error bars are from the fitting uncertainties to obtain the peak position from CT bleaching signals. (f) Formation time of the transient E-field as a function of the excitation fluence, and the error bars come from the exponential fitting uncertainties to extract the build-up dynamics of bleaching signals at the CT minimum.

process in Figure 2c is absent in the redshifting process presented in Figure 2a. (ii) The redshift process with a lifetime of ∼1.21 ps obtained in Figure 2c is more reliable since the accuracy of the dynamic evolution in Figure 2a is limited due to the ignorance for the time-dependent carrier population, a fitting error to determine the energy peak, and the spectra overlapping with the photo-induced absorptions.[36]

After the observation of an ultrafast modulation of the CT transition, we now attempt to figure out the possible mechanism responsible for the blueshift–redshift crossover of CT transitions. Since we do not observe a universal transition shift (i.e., no change of intradomain transitions) at a high excitation density, the measured transition crossover of the CT state with considerable energy shifting should be related to the process at the heterojunction. Also, such a transition crossover of the CT state cannot be due to a combination of those general effects because they would also cause a change of intradomain transitions, such as enhanced Coulombic screening,[37] pump-induced lattice heating,[38] band-gap renormalization,[7] and a Burstein–Moss effect.[39] In addition, we have noticed that the reversible carrier trapping by the structure defects can involve in such a transition crossover. Despite the carrier trapping occurring in the picosecond range, the reversed process (i.e., the carrier releasing) is relatively slow and typically with a lifetime of several microseconds,[40] which is inconsistent with our observation. More interestingly, accompanying the CT transition crossover, the build-up of the intradomain bleaching signals becomes much slower at a high excitation density (see Figure 2a and Figure S4), which is in striking contrast with the fast build-up process at a low excitation fluence (Figure S2). Since two already-known channels that contribute to the build-up of intradomain bleaching signals (i.e., optical excitation and charge transfer) occur on the picosecond timescale, we suggest that, at a high excitation density, there should be a new dynamic process to go against and slow down the ultrafast charge transfer. Hence, carrier separation becomes less efficient or incomplete, leading to the observation of pure domain emission at a high excitation fluence (an emission peak from the CdTe domain emerges in addition to the main type-II emission at ∼9000 $\mu J/cm^2$).[24]

In light of the above discussion, combined with the type-II band alignment in CdSe/CdTe CQWs, the most reasonable hypothesis to interpret the observed CT transition crossover is the formation and dissipation of a transient E-field ($\Delta\varepsilon$) across the interface. As schematically illustrated in Figure 3, the type-II heterostructure in CdSe/CdTe CQWs functions similarly to a p–n junction in photovoltaics or photodectors:[23] At phase I (the carrier transfer process), in the presence of a built-in potential resulting from type-II band offsets, photo-generated hot electrons and holes in one domain are efficiently transferred to the CdSe domain and CdTe domain within one picosecond (∼0.47 ps) and eventually leading to n-doping (p-doping) for CdSe (CdTe). While at phase II (the carrier accumulation process at the crown–core interface), hot carriers diffuse to the hetero-interface and cool down through an interaction with longitudinal optical phonon modes. At this stage, the accumulation of opposite charges across the interface generates a transient $\Delta\varepsilon$ that counteracts the further charge separation driven by the built-in E-field. In other words, the transient electric field will prevent the continuous accumulation of the same charges at one side of the interface, which is very similar to repulsive interactions among same charges.[24,25] Consequently, the conduction band minimum and valence

https://doi.org/10.1021/acsphotonics.2c01799
ACS Photonics 2023, 10, 1250–1258

band maximum near the interface start to bend and subsequently cancel out the initial built-in potential, leading to the blueshift of the CT transition. Please note that the timescale of the blueshifting process in our work (~4 ps) is consistent with the crown-to-core carrier diffusion lifetime (~5 ps) extracted by Pandya et al.[16] and Li et al.[15] It is also worth mentioning that the presence of $\Delta\varepsilon$ at molecular donor/acceptor interfaces[41] or the p−n/Schottky junctions[22] has already been observed and probed via femtosecond optical spectroscopy. Later, at phase III (the CT exciton formation process), the carrier−phonon interaction further localizes the electron−hole pair at the crown−core interface, forming the "cold" CT excitons with a timescale of ~1.21 ps.[16,23] As a result, $\Delta\varepsilon$ disappears due to the formation of neutral excitons, and therefore, the band alignment is restored to the initial scenario. Due to the relatively slow recombination dynamics (see Figure S1; lifetime: >50 ns) in CdSe/CdTe CQWs and the relatively small energy shifting value due to the Burstein−Moss effect (several millielectronvolts with our excitation conditions), we argue that the contribution of the reduced carrier population to the redshift of the CT transition should be negligible. Furthermore, in phase I, these photo-generated electron−hole pairs are more likely to diffuse to the interface in the form of domain excitons and then dissociate into the unbounded carriers due to the presence of a built-in potential since it can avoid the strict parallel momentum conservation, as argued by Mishchenko et al.[42] Here, we have simplified these processes and depicted the unbounded electron−hole pairs only instead of domain excitons for clarity in these schematics. Please note that the above explanation is also supported by the absence of a CT transition crossover when only pumping the lowest-energy CT exciton (see the data in Figures S5 and S6). Without carrier diffusion due to the 590 nm excitation, the transient $\Delta\varepsilon$ (phase II in Figure 3) cannot be built up, leading to a time-independent CT transition energy.

To further prove that the observed CT transition crossover is indeed due to the photo-induced transient $\Delta\varepsilon$, we show that the CT transition characteristics can be gradually modulated by varying the excitation fluence to change the photogenerated carrier density with the strength and dynamics of $\Delta\varepsilon$. Figure 4a−d and Figure S7 show the corresponding two-dimensional plots of the TA spectra for the pump fluences ranging from a relatively low value with which we can barely see the modulation (233 μJ/cm^2, i.e., $\langle N_{e-h}\rangle$: ~40) to the highest value that can be reached in our lab (3649 μJ/cm^2, i.e., $\langle N_{e-h}\rangle$: ~700). We see that there is no energy shifting of intradomain transitions for different carrier densities, which is consistent with our discussion above (also see the extracted peak values in Figures S8 and S9). Similar to our previous analysis in Figure 2c, we have extracted the maximum energy position of the CT transition, the formation, and the dissipation lifetime of $\Delta\varepsilon$ versus excitation fluence. As shown in Figure 4e, the peak energy of CT transition can be well fitted by the equation: $E_p = E_0 + a\cdot F^{1/3}$, where E_0 is the static value and a is a fitting parameter. This cube root dependence on the excitation fluence is in good harmony with the behavior of the $\Delta\varepsilon$-caused band bending predicted theoretically.[43] When approaching the carrier equilibrium (i.e., at the CT transition crossover turning point), the electron density n_e and hole density n_h accumulated at the interface can be related to fluence F as: $n_e\cdot n_h \propto F$. These charged carriers generate an approximately triangular potential well at the heterojunction with the transient $\Delta\varepsilon$ proportional to n_e (i.e., $F^{1/2}$), and the ground state quantization energy in such a triangular potential well is shifted proportionally with $\Delta\varepsilon^{2/3}$. Thus, the band bending energy is expected to increase proportionally with the cubic root of F.

Figure 4f summarizes the measured formation times of $\Delta\varepsilon$, that is, the build-up lifetime of bleaching at the minimum CT transition wavelength, as a function of the excitation fluence. We observe a slower formation process at a higher excitation density (except the first data point in which there is a substantial fitting error due to the subtle CT transition shift with a low excitation fluence). Indeed, because of the strong carrier density dependence of equilibrium conditions, we do expect a prolonged carrier diffusion and accumulation time for a higher pump fluence, and the result in Figure 4f is a necessary consequence of the slower dynamic balance at the heterojunction with a more intensive excitation. While the dissipation lifetime of $\Delta\varepsilon$ exhibits an irregular trend with an increasing fluence (see Figure S10), which, at this stage, is still a puzzle, further studies are required to investigate how electron−hole pairs collapse to the lowest CT state. With low fluences, there is an up-and-down fluctuation for the dissipation time, reflecting a competition among multiple involved processes to form the "cold" CT excitons. With a further increase of a fluence larger than 2164 μJ/cm^2, an accelerated dissipation process of $\Delta\varepsilon$ is observed, which we speculate to be the result of a stronger carrier/phonon interaction to localize the electron−hole pair at a high carrier density (i.e., each domain is more polarized). Another reason could be the contribution of the muti-exciton Auger effect to deplete the carriers. Though the Auger lifetime in type-II CQWs is very slow due to the apparent momentum mismatch in CT excitons,[44] which is the main reason for the excellent optical gain performance,[24] under a high enough fluence as in our experiments, a muti-exciton Auger effect might not be ignored anymore.

CONCLUSIONS

In summary, we have demonstrated for the first time the ultrafast modulation of an indirect transition in type-II colloidal quantum wells by an all-optical approach. The observed blueshift−redshift crossover of the indirect transition energy is closely analogous to the carrier equilibrium process in a p−n junction: the transient E-field created by the separated charges at the heterojunctions opposes the localization process driven by the band offset. Through transient absorption spectroscopy, we have revealed that the formation and decay of the transient E-field occur on the picosecond timescale and are controllable via adjusting the excitation fluence. Our results suggest that type-II colloidal quantum wells with their remarkable optical properties and preferable solution processability hold great promise for the development of novel optical switching and modulators.

METHODS

Materials. Cadmium oxide [CdO] (99.9%), cadmium acetate dihydrate [$Cd(OAc)_2\cdot 2H_2O$] (>98%), myristic acid (>99%), tellurium (Te) (99.99%), selenium (Se) (99.99%), oleic acid (OA) (90%), 1-octadecene (ODE), trioctylphoshine (TOP), hexane, and ethanol (EtOH) were purchased from Sigma-Aldrich.

Synthesis of 4 ML CdSe CQWs. In the typical 4 ML CdSe CQW synthesis, 77 mg of CdO, 340 mg of myristic acid, and 28 mL of ODE were added in a 50 mL round bottom flask, and the solution was degassed at 100 °C. Then, the solution was

https://doi.org/10.1021/acsphotonics.2c01799
ACS Photonics 2023, 10, 1250−1258

heated up to 285 °C under an argon flow until it became a colorless transparent solution, and it was cooled down to 90 °C. In another flask, 24 mg of Se powder was dissolved in 2 mL of ODE using ultrasonication. At 90 °C, the Se precursor solution was injected into the Cd precursor solution, and the temperature was set to 235 °C. After the temperature reached ∼195 °C, 160 mg of $Cd(OAc)_2{\cdot}2H_2O$ was added swiftly. At 235 °C, the reaction was maintained for 10 min, and it was terminated with the addition of a 1 mL OA injection. The NPL solution was cooled down to room temperature using a water bath, and 5 mL of hexane was injected to increase the solubility of NPLs. The obtained CdSe CQW solution was washed with the addition of EtOH at 6000 rpm for 5 min. Precipitates were re-dissolved in hexane.

Synthesis of 4 ML CdSe/CdTe Core−Crown CQWs. For the synthesis of CdSe/CdTe core−crown NPLs, a similar method in the literature was used.[19] In a 50 mL round bottom flask, 1 mL of CdSe NPL solution, 30 mg of $Cd(OAc)_2{\cdot}2H_2O$, 0.45 μL of OA, and 4 mL of ODE were mixed with a magnetic stirrer and degassed at 100 °C. Then, under an argon flow, the temperature was increased to 215 °C, and at this temperature, 0.03 M TOP-Te solution in ODE was injected with a rate of 4 mL/h using a syringe pump. After a certain amount of precursor injection (according to the desired crown size), the reaction was cooled down to room temperature using a water bath and 3 mL of hexane was injected. Products were washed with EtOH addition and centrifuged at 6000 rpm for 5 min. Precipitates were re-dissolved in hexane.

Steady-State Optical Properties of CdSe/CdTe CQWs. Absorption spectra of CQWs in hexane are collected by a UV−vis spectrophotometer (Shimadzu, UV-1800). The PL spectra of CQWs in hexane are recorded using a spectrofluorophotometer (Shimadzu, RF-5301PC; excitation wavelength: 355 nm).

Time-Resolved Photoluminescence of CdSe/CdTe CQWs. Time-resolved PL (trPL) measurements are performed with a streak camera from Optronics. The 400 nm pump laser pulses for trPL are generated from a 1000 Hz regenerative amplifier (Coherent LibraTM). The beam from the regenerative amplifier has a center wavelength at 800 nm and a pulse width of approximately 150 fs and is seeded by a mode-locked Ti-sapphire oscillator (Coherent Vitesse, 80 MHz). The 400 nm pump laser was obtained by frequency-doubling the 800 nm fundamental regenerative amplifier output using a BBO crystal. All measurements are performed in CQWs dispersed in hexane at room temperature in ambient air (53 ± 2% humidity) conditions.

Determination of $\langle N_{e-h}\rangle$ in CdSe/CdTe CQWs. Considering the single-photon pumping regime (i.e., excitation wavelength: 410 nm), we adopt this equation[45] to calculate the number of excitation-generated electron−hole pairs $\langle N_{e-h}\rangle$: $\langle N_{e-h}\rangle = f{\cdot}\sigma/(\hbar\upsilon)$, where f is the pump fluence ($\mu J/cm^2$), σ is the absorption cross-section (cm^2), and $\hbar\upsilon$ is the photon energy (μJ) of the pumping pulse. Here, we calculate σ based on the absorbance data using the method reported by Yu et al.[46] The extracted absorption cross-section at 410 nm is 9.32×10^{-14} cm^2.

Transient Absorption Spectroscopy of CdSe/CdTe CQWs. TA spectroscopy is performed using a Helios setup (Ultrafast Systems LLC) and in the transmission mode with chirp correction. The white-light continuum probe beam (in the range of 400−800 nm) is generated from a 3 mm sapphire crystal using an 800 nm pulse from the regenerative amplifier as mentioned in trPL measurements. The pump beam spot size is ∼0.5 mm. The probe beam passing through the sample was collected using a detector for UV−vis (CMOS sensor). All measurements are performed at room temperature in solution (hexane).

■ ASSOCIATED CONTENT

Data Availability Statement

The raw data and processed data are available via reasonable request to the corresponding authors.

Supporting Information

The Supporting Information is available free of charge at https://pubs.acs.org/doi/10.1021/acsphotonics.2c01799.

Time-resolved PL; Supplemental data of time-resolved absorbance spectroscopy excited at 410 nm; Gaussian fitting results; Time-resolved absorbance spectroscopy excited at 590 nm; The dissipation time of the transient E-field (PDF)

■ AUTHOR INFORMATION

Corresponding Authors

Junhong Yu − *LUMINOUS! Centre of Excellence for Semiconductor Lighting and Displays, School of Electrical and Electronic Engineering, The Photonics Institute (TPI), Nanyang Technological University, 639798, Singapore;* orcid.org/0000-0001-6136-552X; Email: jyu012@e.ntu.edu.sg

Hilmi Volkan Demir − *LUMINOUS! Centre of Excellence for Semiconductor Lighting and Displays, School of Electrical and Electronic Engineering, The Photonics Institute (TPI), Nanyang Technological University, 639798, Singapore; School of Physical and Mathematical Sciences, Division of Physics and Applied Physics, Nanyang Technological University, 639798, Singapore; Department of Electrical and Electronics Engineering and Department of Physics, UNAM-Institute of Materials Science and Nanotechnology, Bilkent University, Ankara 06800, Turkey;* orcid.org/0000-0003-1793-112X; Email: volkan@stanfordalumni.org

Cuong Dang − *LUMINOUS! Centre of Excellence for Semiconductor Lighting and Displays, School of Electrical and Electronic Engineering, The Photonics Institute (TPI), Nanyang Technological University, 639798, Singapore; CINTRA UMI CNRS/NTU/THALES 3288, 637553, Singapore;* orcid.org/0000-0001-6183-4082; Email: hcdang@ntu.edu.sg

Authors

Emek Goksu Durmusoglu − *LUMINOUS! Centre of Excellence for Semiconductor Lighting and Displays, School of Electrical and Electronic Engineering, The Photonics Institute (TPI), Nanyang Technological University, 639798, Singapore; School of Physical and Mathematical Sciences, Division of Physics and Applied Physics, Nanyang Technological University, 639798, Singapore;* orcid.org/0000-0001-6840-8342

Yimeng Wang − *LUMINOUS! Centre of Excellence for Semiconductor Lighting and Displays, School of Electrical and Electronic Engineering, The Photonics Institute (TPI), Nanyang Technological University, 639798, Singapore*

Manoj Sharma − *LUMINOUS! Centre of Excellence for Semiconductor Lighting and Displays, School of Electrical and Electronic Engineering, The Photonics Institute (TPI),*

Nanyang Technological University, 639798, Singapore; ARC Centre of Excellence in Exciton Science, Department of Materials Science and Engineering, Monash University, Melbourne, Victoria 3800, Australia

Complete contact information is available at: https://pubs.acs.org/10.1021/acsphotonics.2c01799

Funding

C.D. thanks the Ministry of Education, Singapore, for the financial support under its AcRF Tier 2 grant (no. MOE-T2EP50121-0012). H.V.D. acknowledges the financial support in part from the Singapore Agency for Science, Technology and Research (A*STAR) MTC program under grant no. M21J9b0085, the Ministry of Education, Singapore, under its Academic Research Fund Tier 1 (no. MOE-RG62/20), and in part from TUBITAK nos. 119N343, 20AG001, 121N395, and 121C266. H.V.D. also acknowledges support from TUBA and TUBITAK 2247-A, National Leader Researchers Program (no. 121C266).

Notes

The authors declare no competing financial interest.

REFERENCES

(1) Haug, H.; Koch, S. W. *Quantum Theory of the Optical and Electronic Properties of Semiconductors;* 4. ed., repr.; World Scientific: New Jersey, NJ, 2005.

(2) Klingshirn, C. F. *Semiconductor Optics;* 1st ed.; Springer, 1997.

(3) Yu, J.; Sharma, M.; Sharma, A.; Delikanli, S.; Demir, H. V.; Dang, C. All-optical control of exciton flow in a colloidal quantum well complex. *Light: Sci. Appl.* **2020**, *9*, 27.

(4) Bassett, L. C.; Heremans, F. J.; Yale, C. G.; Buckley, B. B.; Awschalom, D. D. Electrical Tuning of Single Nitrogen-Vacancy Center Optical Transitions Enhanced by Photoinduced Fields. *Phys. Rev. Lett.* **2011**, *107*, No. 266403.

(5) Yu, J.; Sharma, M.; Wang, Y.; Delikanli, S.; Baruj, H. D.; Sharma, A.; Demir, H. V.; Dang, C. Modulating Emission Properties in a Host−Guest Colloidal Quantum Well Superlattice. *Adv. Opt. Mater.* **2022**, *10*, No. 2101756.

(6) Sun, T. Y.; Tu, J.; Zhou, Z. P.; Sun, R.; Zhang, X. W.; Li, H. O.; Xu, Z. M.; Peng, Y.; Liu, X. P.; Wang, P. H.; Wang, Z. C. Resistive switching of self-assembly stacked h-BN polycrystal film. *Cell Rep. Phys. Sci.* **2022**, *3*, No. 100939.

(7) Deng, B.; Tran, V.; Xie, Y.; Jiang, H.; Li, C.; Guo, Q.; Wang, X.; Tian, H.; Koester, S. J.; Wang, H.; Cha, J. J.; Xia, Q.; Yang, L.; Xia, F. Efficient electrical control of thin-film black phosphorus band gap. *Nat. Commun.* **2017**, *8*, 14474.

(8) Yu, J.; Dang, C. Colloidal Metal Chalcogenide Quantum Wells for Laser Applications. *Cell Rep. Phys. Sci.* **2021**, *2*, No. 100308.

(9) Li, H. O.; Cao, L.; Fu, T.; Li, Q.; Zhang, F. B.; Xiao, G. L.; Chen, Y. H.; Liu, X. P.; Zhao, W. N.; Yu, Z. Q.; et al. Morphology-dependent high antireflective surfaces via anodic aluminum oxide nanostructures. *Appl. Surf. Sci.* **2019**, *496*, No. 143697.

(10) Yu, J.; Shendre, S.; Koh, W. K.; Liu, B.; Li, M.; Hou, S.; Hettiarachchi, C.; Delikanli, S.; Hernández-Martínez, P.; Birowosuto, M. D.; Wang, H.; Sum, T. C.; Demir, H. V.; Dang, C. Electrically control amplified spontaneous emission in colloidal quantum dots. *Sci. Adv.* **2019**, *5*, No. eaav3140.

(11) Diroll, B. T.; Chen, M.; Coropceanu, I.; Williams, K. R.; Talapin, D. V.; Guyot-Sionnest, P.; Schaller, R. D. Polarized NearInfrared Intersubband Absorptions in CdSe Colloidal Quantum Wells. *Nat. Commun.* **2019**, *10*, 4511.

(12) Tanghe, I.; Butkus, J.; Chen, K.; Tamming, R. R.; Singh, S.; Ussembayev, Y.; Neyts, K.; van Thourhout, D.; Hodgkiss, J. M.; Geiregat, P. Broadband Optical Phase Modulation by Colloidal CdSe Quantum Wells. *Nano Lett.* **2022**, *22*, 58−64.

(13) Gollner, C.; Jutas, R.; Kreil, D.; Dirin, D. N.; Boehme, S. C.; Baltuška, A.; Kovalenko, M. V.; Pugžlys, A. Ultrafast Electro-Absorption Switching in Colloidal CdSe/CdS Core/Shell Quantum Dots Driven by Intense THz Pulses. *Adv. Opt. Mater.* **2022**, *10*, No. 2102407.

(14) Wu, K.; Li, Q.; Jia, Y.; McBride, J. R.; Xie, Z. X.; Lian, T. Efficient and ultrafast formation of long-lived charge-transfer exciton state in atomically thin cadmium selenide/cadmium telluride type-II heteronanosheets. *ACS Nano* **2015**, *9*, 961−968.

(15) Li, Q.; Zhou, B.; McBride, J. R.; Lian, T. Efficient diffusive transport of hot and cold excitons in colloidal type II CdSe/CdTe core/crown nanoplatelet heterostructures. *ACS Energy Lett.* **2017**, *2*, 174−181.

(16) Pandya, R.; Chen, R. Y. S.; Cheminal, A.; Dufour, M.; Richter, J. M.; Thomas, T. H.; Ahmed, S.; Sadhanala, A.; Booker, E. P.; Divitini, G.; Deschler, F.; Greenham, N. C.; Ithurria, S.; Rao, A. Exciton-phonon interactions govern charge-transfer-state dynamics in CdSe/CdTe two-dimensional colloidal heterostructures. *J. Am. Chem. Soc.* **2018**, *140*, 14097−14111.

(17) Yu, J.; Hou, S.; Sharma, M.; et al. Strong Plasmon-Wannier Mott Exciton Interaction with High Aspect Ratio Colloidal Quantum Wells. *Matter* **2020**, *2*, 2020.

(18) Li, Q.; Xu, Z.; McBride, J. R.; Lian, T. Low threshold multiexciton optical gain in colloidal CdSe/CdTe Core/Crown type-II nanoplatelet heterostructures. *ACS Nano* **2017**, *11*, 2545−2553.

(19) Kelestemur, Y.; Olutas, M.; Delikanli, S.; Guzelturk, B.; Akgul, M. Z.; Demir, H. V. Type-II colloidal quantum wells: CdSe/CdTe core/crown heteronanoplatelets. *J. Phys. Chem. C* **2015**, *119*, 2177−2185.

(20) Pedetti, S.; Ithurria, S.; Heuclin, H.; Patriarche, G.; Dubertret, B. Type-II CdSe/CdTe Core/Crown Semiconductor Nanoplatelets. *J. Am. Chem. Soc.* **2014**, *136*, 16430−16438.

(21) Zhang, J.; Du, L.; Feng, S.; Zhang, R.-W.; Cao, B.; Zou, C.; Chen, Y.; Liao, M.; Zhang, B.; Yang, S. A.; Zhang, G.; Yu, T. Enhancing and Controlling Valley Magnetic Response in MoS2/WS2 Heterostructures by All-Optical Route. *Nat. Commun.* **2019**, *10*, 4226.

(22) Yang, Y.; Gu, J.; Young, J. L.; Miller, E. M.; Turner, J. A.; Neale, N. R.; Beard, M. C. Semiconductor interfacial carrier dynamics via photoinduced electric fields. *Science* **2015**, *350*, 1061−1065.

(23) Zhu, X.; Monahan, N. R.; Gong, Z.; Zhu, H.; Williams, K. W.; Nelson, C. A. Charge Transfer Excitons at Van Der Waals Interfaces. *J. Am. Chem. Soc.* **2015**, *137*, 8313−8320.

(24) Gao, Y.; Li, M.; Delikanli, S.; Zheng, H.; Liu, B.; Dang, C.; Sum, T. C.; Demir, H. V. Low-Threshold Lasing from Colloidal CdSe/CdSeTe Core/Alloyed-Crown Type-II Heteronanoplatelets. *Nanoscale* **2018**, *10*, 9466−9475.

(25) Scott, R.; Kickhofel, S.; Schoeps, O.; Antanovich, A.; Prudnikau, A.; Chuvilin, A.; Woggon, U.; Artemyev, M.; Achtstein, A. W. Temperature dependent radiative and non-radiative recombination dynamics in CdSe-CdTe and CdTe-CdSe type II hetero nanoplatelets. *Phys. Chem. Chem. Phys.* **2016**, *18*, 3197−3203.

(26) Guzelturk, B.; Kelestemur, Y.; Olutas, M.; Li, Q.; Lian, T.; Demir, H. V. High-Efficiency Optical Gain in Type-II Semiconductor Nanocrystals of Alloyed Colloidal Quantum Wells. *J. Phys. Chem. Lett.* **2017**, *8*, 5317−5324.

(27) Hong, X.; Kim, J.; Shi, S.-F.; Zhang, Y.; Jin, C.; Sun, Y.; Tongay, S.; Wu, J.; Zhang, Y.; Wang, F. Ultrafast Charge Transfer in Atomically Thin MoS_2/WS_2 Heterostructures. *Nat. Nanotechnol.* **2014**, *9*, 682−686.

(28) Wang, S.; Wang, L.-W. Exciton Dissociation in CdSe/CdTe Heterostructure Nanorods. *J. Phys. Chem. Lett.* **2011**, *2*, 1−6.

(29) Zhu, H.; Song, N.; Lian, T. Wave Function Engineering for Ultrafast Charge Separation and Slow Charge Recombination in Type II Core/Shell Quantum Dots. *J. Am. Chem. Soc.* **2011**, *133*, 8762−8771.

(30) Jiao, S.; Shen, Q.; Mora-Sere, I.; Wang, J.; Pan, Z.; Zhao, K.; Kuga, Y.; Zhong, X.; Bisquert, J. Band Engineering in Core/Shell ZnTe/CdSe for Photovoltage and Efficiency Enhancement in Exciplex Quantum Dot Sensitized Solar Cells. *ACS Nano* **2015**, *9*, 908−915.

(31) Jones, M.; Kumar, S.; Lo, S. S.; Scholes, G. D. Exciton Trapping and Recombination in Type Ii Cdse/Cdte Nanorod Heterostructures. *J. Phys. Chem. C* **2008**, *112*, 5423−5431.
(32) Dooley, C. J.; Dimitrov, S. D.; Fiebig, T. Ultrafast Electron Transfer Dynamics in CdSe/CdTe Donor−Acceptor Nanorods. *J. Phys. Chem. C* **2008**, *112*, 12074−12076.
(33) Rivera, P.; Schaibley, J. R.; Jones, A. M.; Ross, J. S.; Wu, S.; Aivazian, G.; Klement, P.; Seyler, K.; Clark, G.; Ghimire, N. J.; Yan, J.; Mandrus, D. G.; Yao, W.; Xu, X. Observation of Long-Lived Interlayer Excitons in Monolayer $MoSe_2$-WSe_2 Heterostructures. *Nat. Commun.* **2015**, *6*, 6242.
(34) Yu, J.; Hu, S.; Gao, H.; Delikanli, S.; Liu, B.; Jasieniak, J. J.; Sharma, M.; Demir, H. V. Observation of Phonon Cascades in Cu-Doped Colloidal Quantum Wells. *Nano Lett.* **2022**, *22*, 10224−10231.
(35) Pelton, M.; Ithurria, S.; Schaller, R. D.; Dolzhnikov, D. S.; Talapin, D. V. Carrier Cooling in Colloidal Quantum Wells. *Nano Lett.* **2012**, *12*, 6158−6163.
(36) Yu, J.; Sharma, M.; Li, M.; Delikanli, S.; Sharma, A.; Taimoor, M.; Altintas, Y.; McBride, J. R.; Kusserow, T.; Sum, T. C.; Demir, H. V.; Dang, C. Low-Threshold Lasing from Copper-Doped CdSe Colloidal Quantum Wells. *Laser Photonics Rev.* **2021**, *15*, No. 2100034.
(37) Yu, J.; Sharma, M.; Li, M.; Liu, B.; Hernandez-Martinez, P. L.; Delikanli, S.; Sharma, A.; Altintas, Y.; Hettiarachchi, C.; Sum, T. C.; Demir, H. V.; Dang, C. Efficient generation of emissive many-body correlations in copper-doped colloidal quantum wells. *Cell Rep. Phys. Sci.* **2022**, *3*, No. 101049.
(38) Sie, E. J.; Steinhoff, A.; Gies, C.; Lui, C. H.; Ma, Q.; Rösner, M.; Schönhoff, G.; Jahnke, F.; Wehling, T. O.; Lee, Y.-H.; Kong, J.; Jarillo-Herrero, P.; Gedik, N. Observation of Exciton Redshift−Blueshift Crossover in Monolayer WS_2. *Nano Lett.* **2017**, *17*, 4210−4216.
(39) Liu, X.; Zhang, Q.; Yip, J. N.; Xiong, Q.; Sum, T. C. Wavelength Tunable Single Nanowire Lasers Based on Surface Plasmon Polariton Enhanced Burstein−Moss Effect. *Nano Lett.* **2013**, *13*, 5336−5343.
(40) Rabouw, F. T.; Kamp, M.; van Dijk-Moes, R. J. A.; Gamelin, D. R.; Koenderink, A. F.; Meijerink, A.; Vanmaekelbergh, D. Delayed Exciton Emission and Its Relation to Blinking in CdSe Quantum Dots. *Nano Lett.* **2015**, *15*, 7718−7725.
(41) Tisdale, W. A.; Williams, K. J.; Timp, B. A.; Norris, D. J.; Aydil, E. S.; Zhu, X. Y. Hot-electron transfer from semiconductor nanocrystals. *Science* **2010**, *328*, 1543.
(42) Mishchenko, A.; Tu, J. S.; Cao, Y.; Gorbachev, R. V.; Wallbank, J. R.; Greenaway, M. T.; Morozov, S. V.; Zhu, M. J.; Wong, S. L.; Withers, F.; Woods, C. R.; Kim, Y.-J.; Watanabe, T.; Taniguchi, T.; Vdovin, E. E.; Makarovsky, O.; Fromhold, T. M.; Falko, V. I.; Geim, A. K.; Eaves, L.; Novoselov, K. S. Twist-controlled resonant tunnelling in graphene/boron nitride/graphene heterostructures. *Nat. Nanotechnol.* **2014**, *9*, 808.
(43) Weisbuch, C.; Vinter, B. *Quantum Semiconductor Structures: Fundamentals and Applications;* 1st ed.; Academic Press: San Diego, CA, 1991.
(44) Piryatinski, A.; Ivanov, S. A.; Tretiak, S.; Klimov, V. I. Effect of quantum and dielectric confinement on the exciton-exciton interaction energy in type II core/shell semiconductor nanocrystals. *Nano Lett.* **2007**, *7*, 108−115.
(45) Yu, J.; Sharma, M.; Delikanli, S.; Birowosuto, M. D.; Demir, H. V.; Dang, C. Mutual Energy Transfer in a Binary Colloidal Quantum Well Complex. *J. Phys. Chem. Lett.* **2019**, *10*, 5193−5199.
(46) Yu, W. W.; Qu, L.; Guo, W.; Peng, X. Experimental determination of the extinction coefficient of CdTe, CdSe, and CdS nanocrystals. *Chem. Mater.* **2003**, *15*, 2854−2860.

https://doi.org/10.1021/acsphotonics.2c01799
ACS Photonics 2023, 10, 1250−1258